Evaluation of nucleic acid binding site of SARS-CoV-2 nucleocapsid as a potential antiviral target using small molecule inhibitors

Preeti Dhaka[1], Ankur Singh[1], Shweta Choudhary[1], Rama Krishna Peddinti[2], Pravindra Kumar*[1], Gaurav Kumar Sharma*[3], Shailly Tomar*[1]

[1] Department of Biosciences and Bioengineering, Indian Institute of Technology Roorkee, Roorkee, Uttarakhand - 247667, India

[2] Department of Chemistry, Indian Institute of Technology Roorkee, Roorkee, Uttarakhand-247667, India

[3] Indian Veterinary Research Institute, Izatnagar, Bareilly, Uttar Pradesh state - 243122, India

Corresponding authors*

***Shailly Tomar**
Professor,
Department of Biosciences and Bioengineering,
Indian Institute of Technology Roorkee,
Uttarakhand (247667), India
ORCID ID: 0000-0002-1730-003X

Email: shailly.tomar@bt.iitr.ac.in

***Gaurav Kumar Sharma**
Senior scientist,
Indian Veterinary Research Institute,
Izatnagar, Bareilly,
Uttar Pradesh state (243122), India
ORCID ID: 0000-0002-9996-9422
Email: gaurvet@gmail.com

***Pravindra Kumar**
Professor,
Department of Biosciences and Bioengineering,
Indian Institute of Technology Roorkee,
Uttarakhand (247667), India
ORCID ID: 0000-0003-2128-7736
Email: pravindra.kumar@bt.iitr.ac.in

Objectives: The study aims to assess binding of small molecules to the RNA binding site of SARS-CoV-2 nucleocapsid protein and evaluate antiviral efficacy of identified inhibitors towards development of new antiviral treatment.
Methods: The N-terminal domain (NTD) of SARS-CoV-2 N protein that binds to viral RNA has been targeted. Atomic structure of NTD was exploited for virtual screening, docking, and MD simulation studies of the identified small molecules that potentially make molecular contacts at the RNA binding site. Molecular interactions of the inhibitory molecules with purified NTD protein were analysed using isothermal titration calorimetry. A plate-based fluorescence protein-RNA interaction assay was used to assess the inhibitory potential of these molecules. Further, *in vitro* cell-based assays evaluated antiviral activity against SARS-CoV-2.
Results: Molecules with high affinity for the target site from compound libraries: FDA-approved, natural product and LOPAC^{1280} that inhibit RNA binding to N-protein were identified using a structure-based *in silico* screening approach. Twelve selected molecules demonstrated significant inhibition of RNA binding with EC50 values of <16 µM. These molecules remarkably inhibited SARS-CoV-2 viral infection in monkey-derived Vero E6 cell lines with an EC_{50} in the low micro molar range. Telmisartan and BMS-189453 were the most potent antivirals with EC_{50} values ~1.0 µM and ~0.98 µM respectively.
Conclusions: The study provides evidence and demonstrates high efficiency of antiviral molecules striving against the RNA binding site of SARS-CoV-2 N-protein of. This is the first study demonstrating antiviral efficacy of repurposed drugs targeting the RNA binding pocket of the NTD of SARS-CoV-2 N protein.

Keywords: SARS-CoV-2, Nucleocapsid, RNA binding domain, Drug repurposing, NTD.

Introduction

Since the beginning of the Coronavirus Disease 2019 (COVID-19) pandemic caused by severe acute respiratory syndrome coronavirus 2 (SARS-CoV-2) virus, attempts are ongoing to develop coronavirus countermeasures. The mRNA vaccines, adenovirus vectors, inactivated viruses, and subunit vaccines are now available, and number of antiviral drugs were used during pandemic to reduce mortality and hospitalization. However, still there is a need for novel effective antivirals to combat emerging variants of SARS-CoV-2 and other emerging coronaviruses[1]. Coronavirus infections including SARS-CoV-2 in humans can cause severe symptoms such as pneumonia, acute respiratory distress syndrome, cytokine storm and organ failure, highlighting the need for effective antiviral therapy[2,3]. The SARS-CoV-2 virus belongs to the Coronaviridae family and has a virion particle consisting of four structural proteins, one of which is the Nucleocapsid (N) protein[4]. The N-protein in SARS-CoV-2 has two functional domains, N-terminal RNA encapsidation domain (NTD; residues 46-174) and the C-terminal oligomerization domain (CTD; residues 247-364), connected by a central linker region, and is involved in regulating viral RNA replication, host cell metabolism, and viral assembly[5,6,7,8]. Research on the SARS-CoV-2 N-protein indicates that the NTD is highly conserved and has structural and functional similarities with other coronaviruses such as the Human coronavirus

OC43 (HCoV-OC43), Mouse hepatitis virus (MHV), MERS, and SARS-CoV[9]. Viral RNA and positively charged NTD form a ribonucleoprotein (RNP) complex through hydrophobic and electrostatic interactions[10]. The crystal structures of NTD-N protein of coronaviruses reveal the RNA binding pocket consisting of Ser52, Phe54, Ala56, Ala91, Arg108, Tyr110, Tyr112, and Arg150 residues, making it a potential target for developing anti-COVID therapeutics. This pocket is responsible for encapsidation of viral RNA and targeting it may disrupt the binding of RNA with the N-protein, affecting gene expression regulation.[11–13]. The process of establishing a new medication on the pharmaceutical market involves costly and time-consuming pre-clinical and clinical trial stages. Efficient screening of existing compound libraries against current and upcoming diseases is crucial to expedite drug discovery and development[14–18]. The drug discovery process can be sped up by using a variety of drug libraries for structure-based screening, biophysical and biochemical validation, and in vitro testing of molecules against target proteins[19–22]. Additionally, the development of a high throughput fluorescence-based protein-RNA binding assay helps in evaluating impact of investigational drugs on molecular interactions and provides a inhibition kinetics method[23,24]. This study aimed to identify small compounds from three different libraries that could potentially target the NTD of SARS-CoV-2 N-protein and inhibit the replication of SARs-CoV-2 virus. Twelve promising molecules were identified through high-throughput drug screening, and their binding affinities and inhibitory effects on NTD-RNA interactions were evaluated using isothermal titration calorimetry and fluorescence intensity-based assays respectively. Ten of these hits showed significant antiviral activity in cell-based investigations. The study provides a strong foundation towards development of antiviral treatment to combat emerging SARs-CoV-2 variants of concern.

Methods

Production of SARS-CoV-2 NTD

The gene fragment of NTD (residues 1-174) was amplified by PCR using the template plasmid received from National Centre for Cell Science (NCCS), Pune (a kind gift from Dr Janesh Kumar). The two sets of oligonucleotide primers 5'-ATATGGCTAGCCGGCCCCAAGGTTTACCCAATAATACTGC-3' (forward) having NheI restriction site & 5'-AAGCTTGTCGACTTATTCTGCGTAGAAGCCTTTTGGCAA-3' (reverse) having SalI restriction site were designed to amplify NTD of N-protein. The PCR product was digested with NheI and SalI enzymes and ligated into the pET28c vector using T4 DNA ligase. The recombinant plasmids were transformed in competent *E. coli* DH5α cells using $CaCl_2$ heat shock method, followed by plasmid isolation and confirmation of the gene insert through DNA sequencing. The recombinant plasmid containing the NTD gene fragment was transformed into the Rosetta (DE3) strain of *E. coli.* The NTD protein was expressed and purified as previously described[11]. The molecular weight and purity of the 6xHis-tagged NTD protein were observed on sodium dodecyl sulphate–polyacrylamide gel electrophoresis (SDS-PAGE). The estimated molecular weight of the protein was 21.7 kDa. The protein was dialysed using 1XPBS buffer (137 mM NaCl, 2.7 mM KCl, 4.3 mM Na_2HPO_4, 1.47 mM KH_2PO_4, pH 7.3) overnight at 4 °C. The protein was concentrated to ~3.6 mg/ml using 10-kDa cut-off Ultra-15 Amicon (Millipore, USA). The protein concentration was estimated using the extension coefficient method at wavelength 280 nm.

Molecular docking of Guanosine monophosphate (GMP) into the RNA binding pocket

Multiple sequence alignment (MSA) of SARS-CoV-2 NTD with the NTD from SARS-CoV, MERS-CoV, and HCoV-OC43 coronaviruses illustrates that the residues involved in interaction with GMP in the RNA binding pocket are primarily conserved. The MSA was done using MultAlin software[25], and the image was processed using ESPript 3.0[26]. To gain deeper insights into the structural similarities of NTD among coronaviruses, the crystal structures downloaded from Protein Data Bank (PDB) were used as a template. The structural superimposition of SARS-CoV-2 (PDB ID: 6M3M)[11] with SARS-CoV (PDB ID: 2OFZ)[27], MERS-CoV (PDB ID: 4UD1)[28], and HCoV-OC43 (PDB ID: 4KJX, 4LI4, 4LM9)[13] was performed using PyMol[29]. For molecular docking study, the atomic structure of SARS-CoV-2 NTD (PDB ID: 6M3M)[11] was retrieved from RCSB-PDB and three-dimensional structure of GMP was extracted from the PubChem database. The protein structure was refined by removing water molecules followed by addition of Kollman charge (8.0) and polar hydrogen atoms. GMP structure was prepared by adding Gasteiger charge (0.5203) and polar hydrogen atoms on it. The refined protein and GMP were further saved in the .pdbqt file. The grid box for docking of GMP was prepared by covering the key RNA binding residues in the NTD of SARS-CoV-2 N-protein (Ser52, Phe54, Ala56, Ala91, Arg108, Tyr110, Tyr112, and Arg150) with dimensions 44Å×46 Å×43Å, and centre point coordinates X= 13.566, Y= -6.239, and Z= -18. The Lamarckian genetic algorithm was used to calculate the 10 conformations of GMP with the maximum number of evaluations (250,000,000) by setting other parameters as default. The AutoDock Tools[30] and AutoDock vina[31] were used for the docking study. The best-fitted conformation of GMP with NTD was carefully picked based on binding energy (B.E.), and root mean square deviation (RMSD) value. The molecular interaction of NTD-GMP complex was evaluated using PyMol[29] and LigPlot[32].

Virtual screening and molecular docking of compound libraries

For structure-based virtual screening of small molecules against NTD, PyRx 0.8[33], and AutoDock tools/Vina[30,31] platforms were used. PyRx 0.8 platform was used to screen the Library of Pharmacologically Active Compounds (LOPAC[1280])[34], Natural compound library[35], and the Food and Drug Administration (FDA) approved drug library[35] against the conserved RNA binding pocket of NTD (PDB ID: 6M3M). Ligands were first energy minimized and then converted from SDF format to Autodock ligands (.pdbqt) format using inbuilt OpenBabel software in PyRx 0.8. Subsequently, the aforementioned grid box dimensions of the NTD-GMP complex were used for virtual screening and molecular docking studies by keeping other parameters as default.

Previous reports showed that the inhibitor (PJ34) against the GMP binding site of NTD of HCoV-OC43 reduced RNA-binding affinity and the viral replication significantly[36,37]. The molecular docking of the best-fit conformation of PJ34 revealed the B.E. -6.2 kcal/mol. Top hit molecules were further selected for detailed docking analyses, using the B.E. of NTD-GMP and NTD-PJ34 complex as a reference. Water molecules were removed from the crystal structure in preparation for molecular docking. The structure of NTD protein was prepared for docking by adding Kollman charges (8.0) and polar hydrogen atoms using AutoDock tools.

The .pdbqt file format of top hit ligands was retrieved from the PyRx directory and processed by adding Gasteiger charges and polar hydrogen atoms. The protein and ligands were saved in .pdbqt file format, and molecular docking of ligands was performed similar to docking of GMP against NTD. The best conformations of the ligands were selected based on interactions with NTD, RMSD values, and their binding energies. The selected NTD-ligand complexes were analysed using PyMOL[29] and LigPlot[+32].

MD simulation of docked NTD-ligand complexes

MD simulation of NTD against the selected 12 molecules was carried out to analyse the related conformational and dynamic changes of NTD and NTD-ligand complexes under physiological conditions. The MD simulation studies with recurrent boundary conditions were carried out using 2022.2 version of the GROMACS program for 100 ns on Linux based workstation. The interacting poses of NTD (PDB ID: 6M3M) and NTD-ligand complexes were obtained using AutoDock Vina 1.2.0[31]. The ligand topology was generated using CHARMM General Force Field (CGenFF)[38] and CHARMM36[39] forcefield parameters were used for all the simulations. The solvation of protein complexes was performed with simple point charge (SPC) within a cubic box. The article mesh Ewald method was used to calculate long-range electrostatic interactions within 10 Å cutoff radius. The steepest descent algorithm was used to minimize the system's energy with a cut-off up to 1000 $kJmol^{-1}$ having 50,000 iteration steps. After the energy minimization process, the system was equilibrated with the following stages; the first phase of equilibration was done under NVT (constant number of particles, volume, and temperature) ensemble followed by NPT (Constant number of particles, pressure, and temperature) ensemble of MD run for 100 ps at 300 K. The positional restrain for covalent bond on heavy protein atoms were equilibrated using LINCS algorithm. MD run was further conducted under NPT conditions where 1 bar pressure was maintained using Parrinello-Rahman barostat, and temperature was regulated within a box by using the V-rescale method (a modified version of Berendsen temperature coupling method). The time of pressure and temperature constants were set as 2 ps and 0.1 ps, respectively. All the trajectories were saved and XMGRACE was used to analyse the results. RMSD in the backbone of protein was calculated using the g rms tool whereas RMSF of protein residues was computed using the g rmsf tool. Rg that is used to measure the compactness factor of the protein was calculated using g gyrate tool and SASA was estimated using gmx sasa, whereas g hbond tool was used to calculate the distance of intermolecular hydrogen bonds within a range of 3.5 Å distance throughout the simulation.

Isothermal Titration Calorimetry (ITC)

ITC experiments were performed using MicroCal ITC_{200} microcalorimeter (Malvern, Northampton, MA)[40] in 1X PBS buffer at 25 °C with reference power 9 µcal/s. Protein and ligands were dissolved in PBS buffer. For NTD-ligands binding experiments, 10-20 µM purified SARS-CoV-2 NTD protein was placed into the cell and ligands in the range of 100-400 µM were filled in the syringe. After equilibration, a total 20 injections of syringe samples were titrated in the cell with one injection of 0.4 µL followed by 19 injections of 2 µL at an

interval of 220 sec. The one-site binding model analysed the binding parameters to obtain ΔH, ΔS, and K_D values using Malvern's Origin 7.0 Microcal-ITC200 analysis software.

Fluorescence intensity-based NTD-RNA binding assay

The fluorescence intensity-based binding assay was performed to characterize the binding of NTD with RNA and to assess the inhibitory potential of identified compounds. For this purpose, fluorescently labelled RNA (5´6-FAM-labeled (UCUCUAAACG) 10-mer RNA) was procured from Biotech Desk Pvt Ltd, India[41] and reconstituted in DEPC treated nuclease free water. The binding buffer (20 mM HEPES, pH-7.0, and 100 mM NaCl) was prepared in DEPC-treated RNAase-free water. The purified NTD protein in range of 0 µM -10 µM was added into 96-well black flat bottom Polystyrene microplates (Corning #3881) followed by 1 nM RNA to each well. Wells containing only RNA were treated as blank controls whereas the wells having non-binding protein (Mpro) with RNA were treated as negative control and the plates were incubated at 4 ˚C for 30 min. The fluorescence intensity was measured on a Synergy HTX multimode plate reader[42] (Agilent BioTek) using Gen5 software at an excitation wavelength of 485/20nm and emission wavelength of 528/20nm with read height 8.5mm. The developed protocol was also applied to study the inhibitory effect of identified compounds against the NTD. To carry out these experiments, compounds at different concentrations were incubated with 5 µM of purified NTD protein for overnight at 4 ˚C. Post incubation, the mixture was transferred to 96-well black flat bottom polystyrene microplates and RNA at a concentration of 1 nM was added to pre-incubated NTD-inhibitor mixture and incubated the plate for 30 min at 4 ˚C. Wells containing RNA with NTD protein were considered as positive controls and wells with only RNA served as negative controls. Fluorescence intensities were measured using plate reader and percentage inhibition vs concentration graphs for binding NTD to RNA were plotted using Graph Pad Prism[43]. The data represents the average from a duplicate set of reactions.

Cell culture and virus preparation

Vero cells were cultured in Eagle's minimum essential medium (EMEM; MP Bio), supplemented with 10% Fetal Bovine Serum (FBS; Himedia), 1 µg/ml Gentamycin (Himedia). Cells were maintained and grown in a humidified atmosphere at 37 °C and 5% CO_2. SARS-CoV-2/Human/IND/CAD1339/2020 (an isolate from a SARS-CoV-2 patient in India) was propagated, stored and titrated using Vero cells. The virus isolate was genetically characterized by whole genome sequencing (GenBank accession no: MZ203529) and was passaged in Vero cells. Briefly, virus stocks were prepared by adding the virus to a confluent monolayer of Vero cells for two days until cytopathic effect (CPE) was observed. The supernatant was collected and clarified by low-speed centrifugation prior to being aliquoted for storage at -80 °C. The titer of virus stock was determined as 50% tissue culture infectious dose **(**$TCID_{50}$/ml) in the confluent monolayer of Vero cells in 96-well plate. The virus titer was determined as $1X10^{6.74}$ $TCID_{50}$/mL. All studies on infectious SARS-CoV-2 were performed in a Biosafety level 3 facility at Indian Veterinary Research Institute (IVRI), Izatnagar Bareilly, after obtaining necessary approvals from Biosafety Committees.

Assessment of cell viability

MTT assay was used to assess the cytotoxic effects of compounds on Vero cells[44]. Briefly, 1×10^4 cells/well were seeded in a 96-well cell culture plate and were allowed to attach for 24 h at 37 °C and 5% CO_2. At confluency of ~80%, the media was removed from all wells, and the cells were washed with sterile PBS. Subsequently, the cells were treated with increasing concentrations of compounds dissolved in 2% EMEM media for 48 h at 37 °C and 5% CO_2. Post incubation, MTT [3-(4,5-dimethylthiazol-2-yl)-2,5-diphenyl tetrazolium bromide] (0.5 mg/ml) was added to each well followed by an incubation period of 4 h at 37 °C and 5% CO_2 in the dark. After incubation, the media was removed from all wells, and the blue formazan crystals were then dissolved in Dimethyl sulfoxide (DMSO, 100 uL/well). Absorbance was measured at 570 nm using a multimode plate reader. Values represent the mean, and error bars denote the standard deviation from duplicate reactions. Cell viability was calculated as a percentage against the untreated control, and the data were plotted using GraphPad Prism to calculate the 50% cytotoxic concentration (CC_{50}) of identified compounds.

Assessment of the antiviral potential of compounds against NTD

For the antiviral assay, 70-80% confluent Vero cells were incubated with various dilutions of compounds in 2% EMEM for 2 h at 37 ºC at 5% CO_2 tension. After incubation, the cells were washed with PBS and were infected with SARS-CoV-2 at 0.01 Multiplicity of infection (MOI) in media without FBS and again incubated for 2 h. The media was subsequently removed after incubation, and a fresh medium containing different concentrations of candidate compounds were added to the respective wells. The plate was incubated for 48 h for assessment of CPE. Following this, 100 µL of cell culture supernatant was harvested for viral RNA extraction using the TRU-PCR viral RNA extraction kit (BlackBio) according to the manufacturer's instructions. Quantitative real-time RT-PCR (qRT-PCR) was carried out using the commercial COVISure-COVID-19 Real-Time PCR kit (Genetix) as per the manufacturer's instructions to quantify the virus yield as described previously[45,46]. A reference drug, hydroxychloroquine was used as a positive control. Percentage inhibition versus concentration graph was plotted, and half maximal effective concentration (EC_{50}) values were calculated using the non-linear regression fit model of GraphPad Prism. Data are represented as mean, and error bars correspond to the standard deviation for a duplicate set of reactions.

Quantification of the antiviral potential of selected compounds by endpoint titration

The antiviral potential of selected compounds was further evaluated by $TCID_{50}$/ml, and virus titers were established by Reed and Muench method[47]. For this purpose, Vero cells were seeded in a 96-well cell culture plate and were incubated at 37 ºC and 5% CO_2 tension overnight. 10-fold serial dilution of cell-culture supernatant samples (compound treated) collected 48 hours post-infection (hpi) of the antiviral assay were used to infect confluent monolayer of Vero cells in 96-well plate (50 uL/well). Untreated virus stock samples were used as the positive control, and samples with only cell-culture media were used as negative control to infect cells. The plate was incubated for 72 h at 37 ºC and 5% CO_2 and monitored for the presence and absence of CPE. Following the incubation period, the media was discarded and the cells were fixed with 10% paraformaldehyde for 6-8 h at room temperature. After fixation, the cells were stained with 0.5% crystal violet. The dilution at which 50% of cells were infected

was calculated, and the data is reported as $\log_{10}$ $TCID_{50}$/ml. The Titer of the virus produced from compound-treated cells and control cells is presented as $TCID_{50}$/ml.

Results

Structure-based identification of NTD inhibitors

The crystal structures of the NTD in complex with several ligands, including GMP from SARS-CoV and PJ34 inhibitor from HCoV-OC43, assisted in the identification of the druggable RNA binding pocket of coronaviruses[13,27,28,48]. Comparative sequencing analysis showed that the RNA binding pocket in the NTD of SARS-CoV-2 N-protein is highly conserved among other members of Coronaviridae family, as indicated in the supplementary figure S1a. Structural alignment of selected coronaviruses NTD structures in complex with GMP, PJ34 inhibitor, and Adenosine monophosphate (AMP) binding sites superimposition also confirms the spatial conservation of the key residues of RNA binding pocket shown in figure S1b-e.

Based on these sequence and structural comparisons, molecular docking of GMP targeting the RNA binding residues (Ser52, Phe54, Ala56, Tyr110, Tyr112, and Arg150) of SARS-CoV-2 NTD was performed using AutoDock Vina[31] and AutoDock Tools[30]. Detail molecular interaction analysis using PyMol and LigPlot^{+} shows the participation of Ala56 and Tyr112 in H-bond formation with GMP, and Ala51, Ser52, Thr55, Ala91, Arg108, Tyr110, and Arg150 residues were found to interact with GMP through hydrophobic interactions in figure 1. The observed binding energy (B.E.) of the NTD-GMP complex was -5.9 kcal/mol. Furthermore, this complex's B.E. was used as a guide to filter and elect potential small molecules from the compound libraries for *in silico* screening studies.

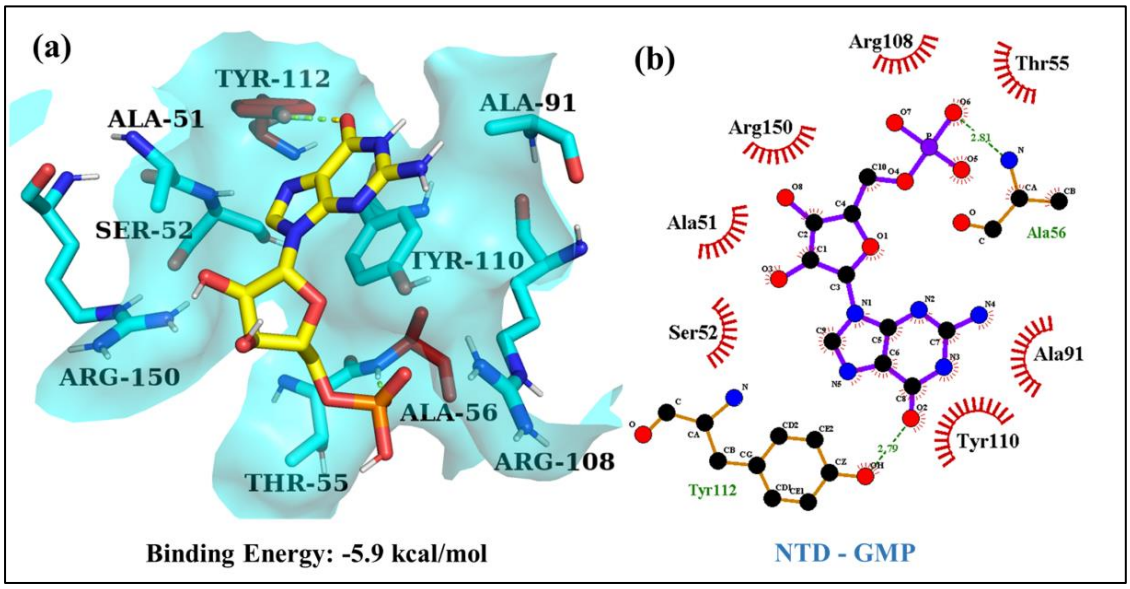

Figure 1. Detailed schematic representation of NTD-GMP complex. (**a)** Three-dimensional molecular interaction analysis of GMP with RNA binding pocket of SARS-CoV-2 NTD was shown using PyMol[29]. Sticks represent the residues of the NTD interacting with GMP are represented using sticks. NTD amino acid residues are shown by red and cyan while GMP is in yellow. The surface covered by interacting residues is indicated by cyan colour with 60% transparency. Red-coloured residues Ala56 and Tyr112 show H-bond interactions, while cyan-coloured stick residues Ala51, Ser52, Thr55, Ala91, Arg108, Tyr110, and Arg150 of NTD show hydrophobic interactions with GMP. The yellow-coloured dotted line guides h-bond interactions. (**b)** Molecular

interactions in SARS-CoV-2 NTD-GMP complex in 2D schematic view analysed using LigPlot+[32]. GMP is represented in purple sticks, while the residues of NTD involved in H-bond interactions are displayed as brown-coloured sticks and green-coloured dotted lines show their H-bond lengths. The red stellate residues represent hydrophobic interactions.

Computer-aided virtual screening of three different libraries was performed to identify potential antivirals against the RNA binding pocket of NTD using PyRx 0.8[33]. After comparing the B.E. with the NTD-GMP complex, top twelve screened compounds were then subjected to molecular docking studies to better investigate the interactions between the NTD and ligands.

Molecular docking and analysis of selected compounds

The compounds that were selected from *in silico* screening of compound libraries were docked into the GMP binding pocket of NTD using AutoDock Vina and AutoDockTools. The B.E. of these compounds was in the range of -6.8 to -7.9 kcal/mol, which is significantly higher than the B.E. of NTD-GMP (-5.9 kcal/mol) in Figure 1. The interactions and binding conformations of the selected small molecules in the RNA binding pocket of NTD indicate that the essential residues involved in binding to GMP or RNA also involved in binding to these molecules shown in Figure 2 and 3. The comparative study of docked NTD-ligand complexes against NTD-GMP complexes reveals the inclusion of extra RNA binding pocket residues that are not involved in GMP binding but are in charge of enhancing interactions between the target protein and the ligand [Table 1].

Table 1. Molecular docking of screened compounds against the nucleotide-binding site of NTD protein provides detailed information about the values of binding energy (kcal/mol), H-bond interactions & hydrophobic interactions. Here, additional residues are underlined and highlighted.

Compound	Binding Energy (kcal/mol)	H-Bond Interactions		Hydrophobic Interactions
		No. of bonds	Residues	
FDA Approved compounds				
BMS-927711	-7.9	1	Tyr110	Thr50, Ala51, Thr55, Ala56, Ala91, Arg108, Tyr112, Pro118, Arg150, Ala157
Telmisartan (MICARDIS)	-7.6	2	Ser52, Tyr112	Ala51, Thr55, Ala56, Ala91, Arg108, Tyr110, Arg150, Pro152, Ala156, Ala157
Bictegravir	-7.5	6	Ser52, Arg89,	Ala51, Tyr110, Pro118

			Tyr112, Arg150	
Natural compounds				
Alisol_B	-7.6	2	Thr50, Arg150	Ala51, Thr55, Arg89, Ala91, Tyr110, Tyr112, Pro118, Ala157
Apatinib	-7.4	1	Arg89	Thr55, Ala56, Ala91, Arg108, Tyr110, Tyr112, Arg150, Ala157
Nomilin	-7.1	4	Ala56, Arg150, Ala157	Thr50, Thr55, Tyr110, Pro152
LOPAC compounds				
ANA-12	-7.4	2	Tyr110, Arg150	Ala51, Ser52, Phe54, Thr55, Ala56, Ala91, Arg108, Tyr112, Ala157
Galloflavin Potassium	-7.2	9	Ser52, Arg90, Arg89, Tyr112, Arg150	Ala51, Ala91, Tyr110
BMS-189453	-6.9	2	Arg89, Tyr112	Thr55, Ala56, Ala91, Tyr110, Arg150, Asn151, Pro152, Ala157
MCC-555	-6.9	3	Arg89, Tyr112, Arg150	Ser52, Thr55, Ala56, Ala91, Tyr110, Pro118
Bisdemethoxycurcumin	-6.8	3	Arg89, Arg150	Ala51, Ser52, Thr55, Ala56, Arg108, Tyr110, Tyr112, Pro118, Ala174
Icilin	-6.8	3	Arg89, Tyr112, Arg150	Thr50, Ala51, Ser52, Thr55, Ala91, Tyr110, Ala157

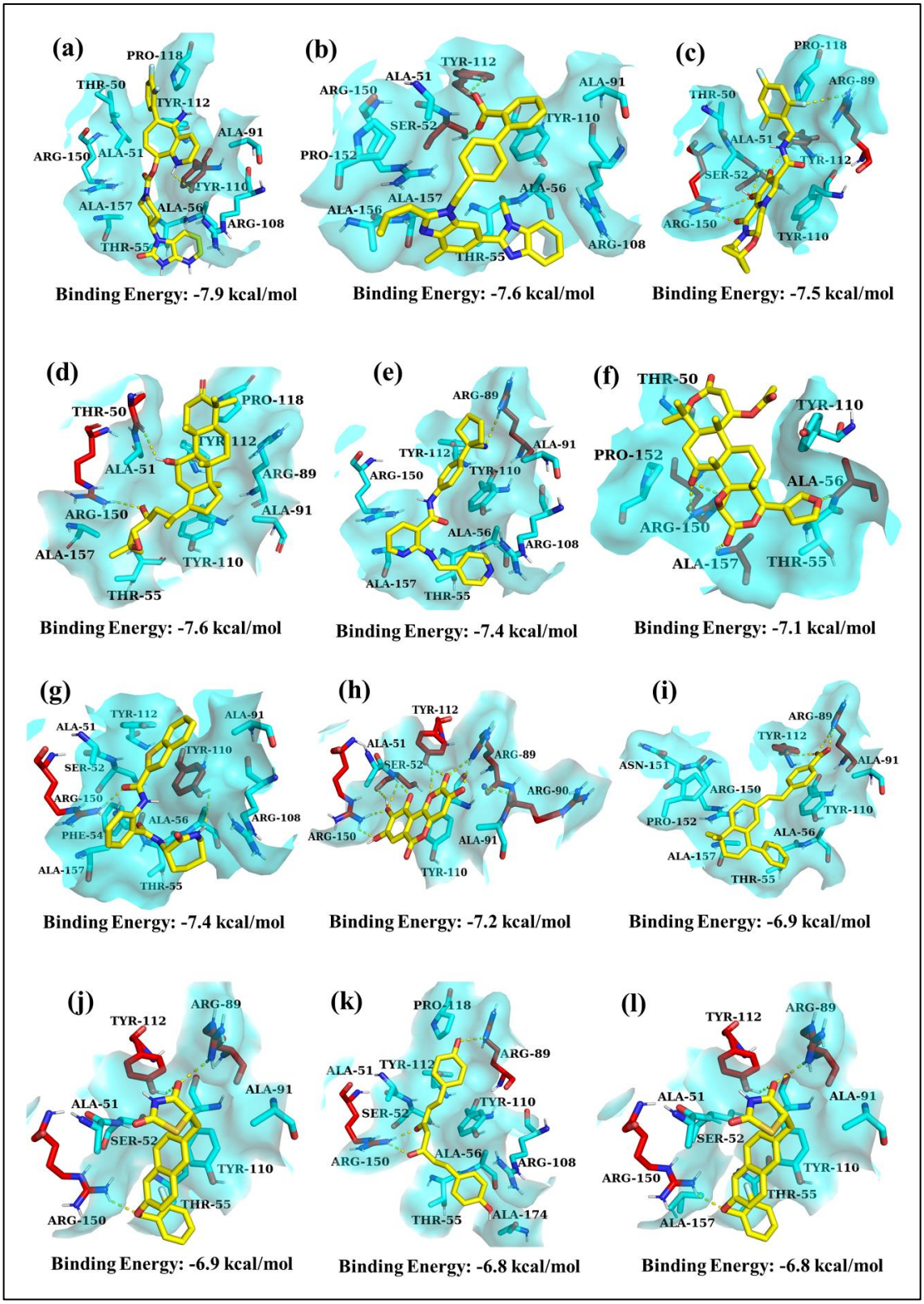

Figure 2. Molecular interaction of compounds in the RNA binding pocket of SARS-CoV-2 NTD. (a) BMS-927711, **(b)** Telmisartan (MICARDIS), **(c)** Bictegravir, **(d)** Alisol_B, **(e)** Apatinib, **(f)** Nomilin,. **(g)** ANA-12, **(h)** Galloflavin_Potassium, **(i)** BMS-189453, **(j)** MCC-555, **(k)** Bisdemethoxycurcumin, and **(l)** Icilin occupy the binding site in the similar manner as GMP. Ligands are shown in yellow coloured sticks, whereas the interacting residues of NTD are represented by cyan and red coloured sticks. The surface covered by interacting residues is

indicated by cyan colour with 60% transparency. The residues involved in H-bond interactions are shown in red-coloured sticks, and residues involved in hydrophobic interactions are involved in cyan-coloured sticks. Yellow-coloured dotted lines show the intermolecular H-bond interactions.

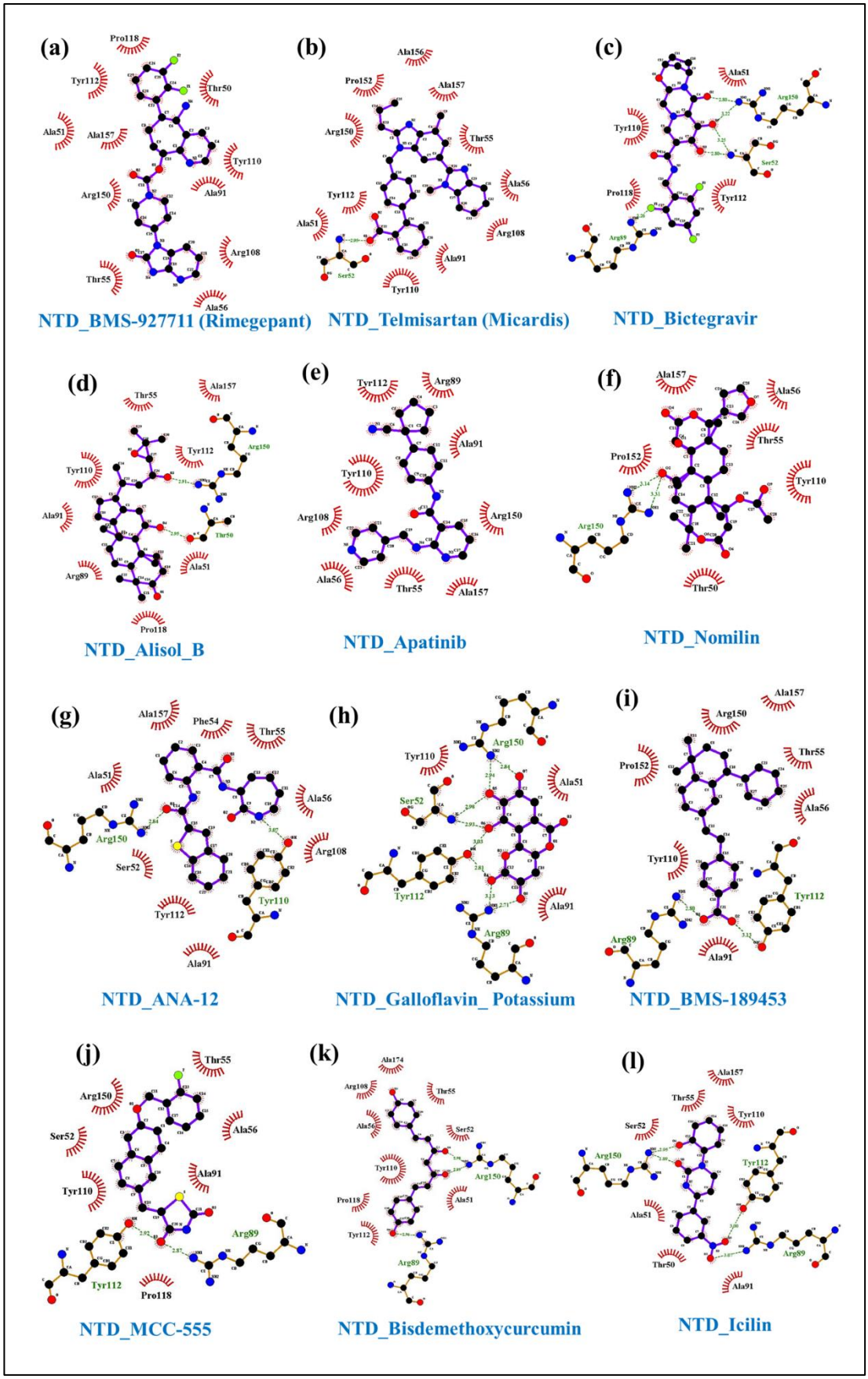
(a)
Pro118
Tyr112
Thr50
Ala51
Ala157
Tyr110
Arg150
Ala91
Arg108
Thr55
Ala56
NTD_BMS-927711 (Rimegepant)
(b)
Ala156
Pro152
Ala157
Arg150
Thr55
Ala56
Tyr112
Ala51
Arg108
Ala91
Ser52
Tyr110
NTD_Telmisartan (Micardis)
(c)
Ala51
Arg150
Tyr110
Ser52
Pro118
Tyr112
Arg89
NTD_Bictegravir
(d)
Thr55
Ala157
Tyr112
Arg150
Tyr110
Ala91
Thr50
Ala51
Arg89
Pro118
NTD_Alisol_B
(e)
Tyr112
Arg89
Ala91
Tyr110
Arg108
Arg150
Ala56
Thr55
Ala157
NTD_Apatinib
(f)
Ala157
Ala56
Thr55
Pro152
Tyr110
Arg150
Thr50
NTD_Nomilin
(g)
Ala157
Phe54
Thr55
Ala51
Ala56
Arg150
Arg108
Ser52
Tyr110
Tyr112
Ala91
NTD_ANA-12
(h)
Arg150
Tyr110
Ala51
Ser52
Tyr112
Ala91
Arg89
NTD_Galloflavin_ Potassium
(i)
Ala157
Arg150
Thr55
Pro152
Ala56
Tyr110
Tyr112
Arg89
Ala91
NTD_BMS-189453
(j)
Thr55
Arg150
Ser52
Ala56
Ala91
Tyr110
Arg89
Tyr112
Pro118
NTD_MCC-555
(k)
Ala174
Arg108
Thr55
Ala56
Ser52
Tyr110
Arg150
Pro118
Ala51
Tyr112
Arg89
NTD_Bisdemethoxycurcumin
(l)
Ala157
Thr55
Tyr110
Ser52
Arg150
Tyr112
Ala51
Thr50
Arg89
Ala91
NTD_Icilin

Figure 3. Molecular interactions in SARS-CoV-2 NTD-compound complexes in 2D schematic view analysed using LigPlot+. Ligands are represented in purple coloured sticks. The residues of NTD involved in hydrophobic interactions are marked as semi-circled red colour, brown colour sticks represent residues involved in intermolecular H-bond interactions, and green coloured dotted lines show their bond lengths.

The residues within the NTD play a critical role in its interaction with ligands. These residues include Ala51, Ser52, Thr55, Phe54, Ala56, Thr58, Ala91, Arg108, Tyr110, Tyr112, Arg150, Ala157, and Ala174. By forming key interactions, these residues can facilitate the binding and stabilization of ligands within the NTD-N protein [Figure 3, 4 and Table 1]. FDA-approved compounds BMS-927711 interacts with one H-bond (Tyr110), Telmisartan interacts with NTD by forming two H-bonds (Ser52 and Tyr112), and Bictegravir shows six H-bonds, with four residues Ser52, Arg89, Tyr112, and Arg150. Natural product compounds Alisol_B interacts with two H-bonds (Thr50 and Arg150), Apatinib with one H-bond (Arg89), and Nomilin displays four H-bonds with residue Ala56, Arg150, and Ala157. LOPAC[1280] compounds ANA-12 interacts with two H-bonds (Tyr110 and Arg150), Galloflavin_Potassium forms nine H-bonds with residues Ser52, Arg89, Arg90, Try112, and Arg150, BMS-189453 with two H-bonds (Arg89 and Tyr112), MCC-555, and Icilin forms three H-bonds with residues Arg89, Tyr112, and Arg150, and Bisdemethoxycurcumin forms three H-bonds with residues Arg89 and Arg150 [Figure 3, 4 and Table 1]. To further validate the binding of the selected small molecules to the NTD-N protein, MD simulations were performed.

MD simulation analysis of docked compounds with NTD

MD simulation investigations were utilised to understand the changes in the stability of protein-ligand complexes at their atomic level. Here, various metrics, including root mean square deviation (RMSD), root mean square fluctuation (RMSF), radius of gyration (Rg), solvent accessible surface area (SASA), and intermolecular H-bonds were examined for 100 ns. The RMSD values represent the change in dynamic conformation in the protein backbone. The majority of the NTD-ligand complexes reach stability within 5-10 ns of simulation and sit within a range of 0.2 to 0.6, according to the analysis of the RMSD value of the NTD-ligand complexes in the current research, as shown in figure S2a. This analysis demonstrates that ligand interactions with the nucleotide-binding pocket are stable and do not affect the stability of protein backbone structure. The RMSF values determine the fluctuation of the polypeptide chain as per C/span> atom coordinates from the reference position at the time of simulation. The RMSF results of complexes in figure S2b showed higher peaks from residues 50-70 are loop regions that is expected to promote the entry of ligands to the RNA binding pocket of NTD. According to the RMSF findings, NTD-ligand complexes have constant atomic mobility; as a result, ligands can form stable complexes with NTD and, thus, prevent the binding of RNA to its pocket. The highly stable protein will exhibit increased compactness since Rg is primarily employed to compute the distances between mass centres and the terminals of protein atoms. In the current study, the Rg plots showed that NTD-ligands complexes have the comparable density to the NTD protein, as shown in figure S 2c. SASA is used to determine the solvation-free energy of every atom of the protein. The rise in the SASA plot suggests the conformational changes in the loop regions because of the presence of hydrophobic residues. SASA plots of NTD-ligand complexes are equivalent to the NTD protein as shown in figure S2d. The number

of H-bonds and their distribution pattern was used to analyse the stability of NTD-ligand complexes throughout the simulation. Moreover, the number of H-bonds increases with time, which represented that the system is attaining stability during simulation time, as shown in figure S2e.

The results of the MD simulations provided additional evidence supporting the specific interactions identified through the PyMol and LigPlot+ analyses. Furthermore, the binding of the selected small molecules has been validated by conducting ITC experiments using purified SARS-CoV-2 NTD of N protein.

Thermodynamic binding analysis of inhibitors to NTD

To determine the binding of selected compounds to the target protein, the thermodynamic binding titration experiments were performed using MicroCal ITC_{200} microcalorimeter (Malvern, Northampton, MA) at 25 °C. The compounds and protein were diluted in 1X PBS buffer at pH 7.3. Ten compounds (except Galloflavin_Potassium and Alisol_B) were titrated at a concentration of 200 µM (in syringe) against 20 µM NTD (in cell). Galloflavin_Potassium was titrated at a concentration of 400 µM by keeping all other parameters same and the remaining compound Alisol_B was titrated at a concentration of 100 µM (in syringe) against 10 µM NTD protein (in cell). ITC isotherms were jointly fit using a one-site binding model for the non-linear curve to determine the thermodynamic parameters such as n, K_D, ΔH, and ΔS. The data were analysed using commercially available Origin7.0 associated with Microcal-ITC200 analysis Software. ITC analysis yielded excellent equilibrium dissociation constant [Figure 4 and Table 2].

Table 2. The thermodynamic analysis of top hit compounds with NTD protein as obtained from ITC.

Protein	**Ligand**	**n**	***K_D* (µM)**	**K_A(M^{-1})**	**ΔH(cal/mol)**	**ΔS(cal/mol/degree)**
NTD	BMS-927711 (Rimgepant)	1	13	$(7.65\pm1.14)10^4$	$(-17.70\pm1.871)10^4$	-571
NTD	Telmisartan (MICARDIS)	1	44.20	$(2.26)10^4\pm561$	$(-2.549)10^5\pm3787$	-835
NTD	Bictegravir	1	22	$(4.52)10^4\pm(3.64)10^3$	$(-6.567)10^4\pm2483$	-199
NTD	Alisol_B	1	5.95	$(1.68)10^5\pm(3.83)10^4$	$(-3.521)10^5\pm(2.920)10^4$	$(-1.16)10^3$
NTD	Apatinib	1	21.69	$(4.61\pm1.20)10^4$	$(-2.166)10^4\pm1977$	-51.3
NTD	Nomilin	1	90	$(1.11)10^4\pm312$	$(-1.379)10^5\pm2796$	-444
NTD	ANA-12	1	40.40	$(2.47)10^4\pm712$	$(-1.819)10^5\pm3054$	-590
NTD	Galloflavin_Potassium	1	36	$(2.72)10^4\pm(1.67)10^3$	$(-2.010)10^5\pm6238$	-654

NTD	BMS-189453	1	39.21	$(2.55)10^4 \pm 711$	$(-4.090)10^5 \pm 6604$	$(-1.35)10^3$
NTD	MCC-555	1	27.4	$(3.65)10^4 \pm (1.06)10^3$	$(-3.024)10^5 \pm 4464$	-993
NTD	Bisdemethoxycurcumin	1	82.6	$(1.21)10^4 \pm 384$	$(-1.632)10^5 \pm 3675$	-529
NTD	Icilin	1	26	$(3.83)10^4 \pm (5.70)10^3$	$(-45.66 \pm 3.300)10^4$	$(-1.51)10^3$

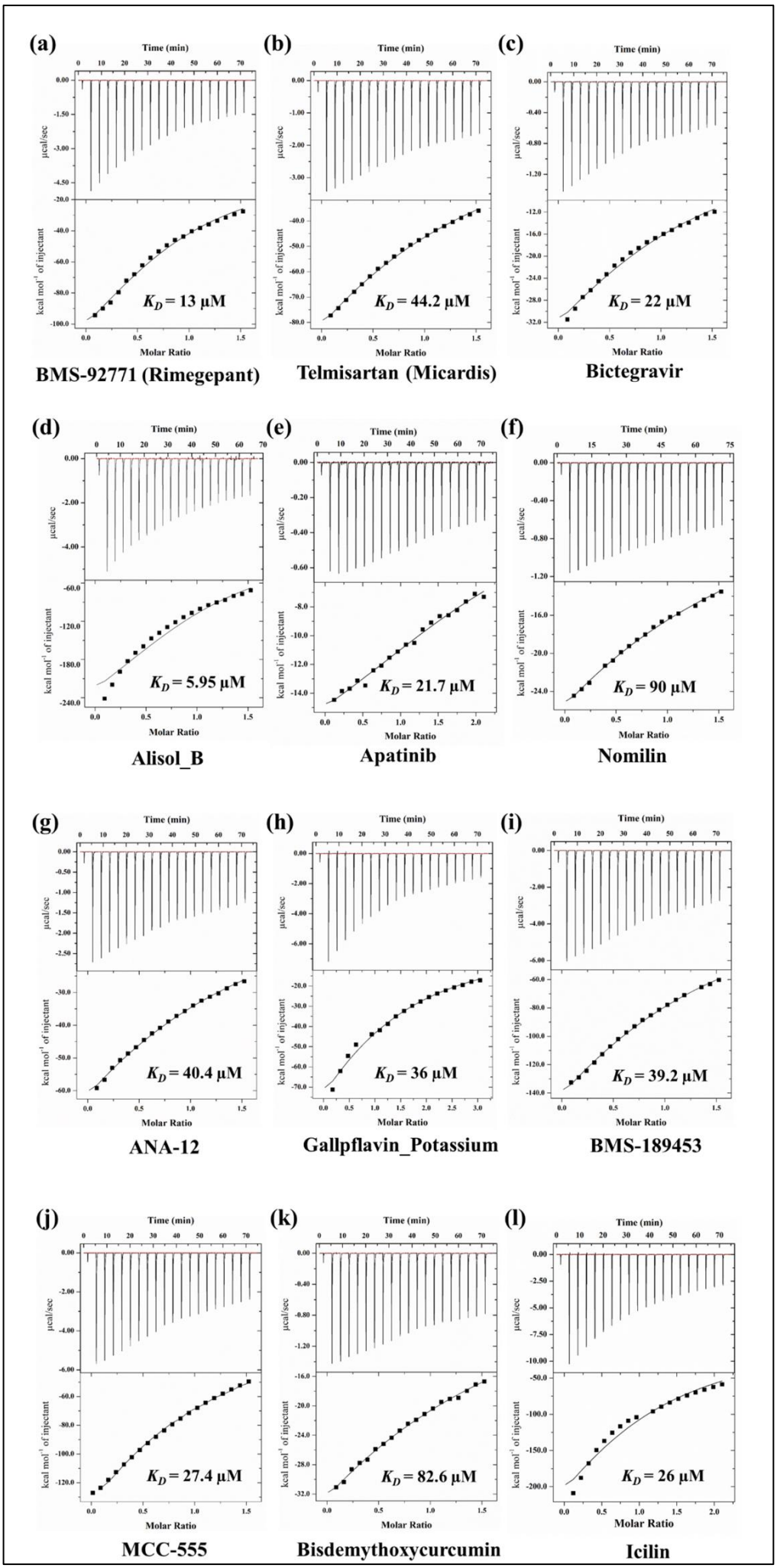
(a)
Time (min)
μcal/sec
kcal mol⁻¹ of injectant
Molar Ratio
K_D = 13 μM
BMS-92771 (Rimegepant)
(b)
Time (min)
μcal/sec
kcal mol⁻¹ of injectant
Molar Ratio
K_D = 44.2 μM
Telmisartan (Micardis)
(c)
Time (min)
μcal/sec
kcal mol⁻¹ of injectant
Molar Ratio
K_D = 22 μM
Bictegravir
(d)
Time (min)
μcal/sec
kcal mol⁻¹ of injectant
Molar Ratio
K_D = 5.95 μM
Alisol_B
(e)
Time (min)
μcal/sec
kcal mol⁻¹ of injectant
Molar Ratio
K_D = 21.7 μM
Apatinib
(f)
Time (min)
μcal/sec
kcal mol⁻¹ of injectant
Molar Ratio
K_D = 90 μM
Nomilin
(g)
Time (min)
μcal/sec
kcal mol⁻¹ of injectant
Molar Ratio
K_D = 40.4 μM
ANA-12
(h)
Time (min)
μcal/sec
kcal mol⁻¹ of injectant
Molar Ratio
K_D = 36 μM
Gallpflavin_Potassium
(i)
Time (min)
μcal/sec
kcal mol⁻¹ of injectant
Molar Ratio
K_D = 39.2 μM
BMS-189453
(j)
Time (min)
μcal/sec
kcal mol⁻¹ of injectant
Molar Ratio
K_D = 27.4 μM
MCC-555
(k)
Time (min)
μcal/sec
kcal mol⁻¹ of injectant
Molar Ratio
K_D = 82.6 μM
Bisdemythoxycurcumin
(l)
Time (min)
μcal/sec
kcal mol⁻¹ of injectant
Molar Ratio
K_D = 26 μM
Icilin

Figure 4. Binding isotherms of identified compounds using ITC: Thermodynamic profiles of ligands against the purified SARS-CoV-2 NTD protein.

The titration curves suggest that the selected compounds bound to NTD of SARS-CoV-2 N-protein with suitable binding constants. A fluorescence intensity-based RNA binding inhibition assay was then carried out to determine the effectiveness of drugs in inhibiting the targeted molecular interactions of RNA with the NTD of N-protein.

Fluorescence intensity-based NTD-RNA binding assay

The molecular interaction of RNA with purified NTD protein and the inhibitory activity of compounds against these molecular interactions was determined by developing and using fluorescence intensity-based NTD-RNA binding assay. The measured fluorescence intensity is directly proportional to the concentration of NTD protein, titrated with 1nM of FAM-labelled RNA as shown in supplementary figure S3. Compounds with the NTD-RNA binding inhibitory capacity leads to decrease in the fluorescence intensity value than that of the free fluorescent RNA because of direct inhibition of NTD-RNA complex formation. The half maximal inhibitory concentration (IC_{50}) of twelve compounds was analysed using GraphPad Prism software. The calculated IC_{50} values for compounds are able to significantly inhibit NTD-RNA interactions [Figure 5]. Hence, the selected antiviral molecules were shown to disrupt the binding interactions of fluorescently labelled RNA with the partner protein NTD.

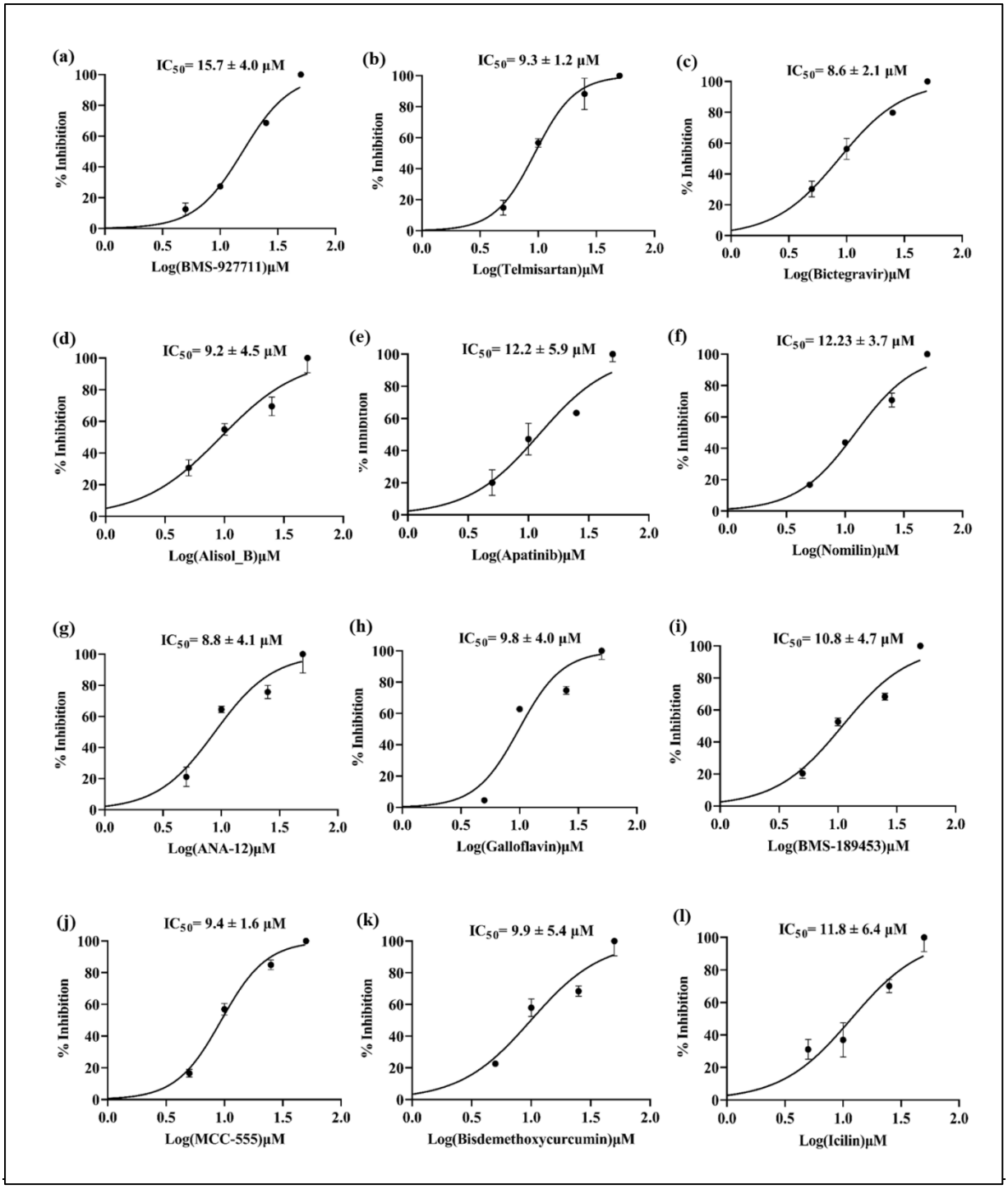

Figure 5. Fluorescence intensity-based NTD-RNA binding assay. The dose-response curves of the NTD-RNA binding inhibition assay involved incubating a fixed concentration of 5µM NTD and 1nM RNA with varying concentrations of compounds. Graph for percentage inhibition of NTD-RNA binding versus the concentrations of compounds plotted using GraphPad Prism software. Error bars represent the standard deviation from duplicate measurements. The results are average of duplicate measurements.

The obtained IC_{50} values suggest that the chosen compounds have excellent binding inhibition for the NTD of the SARS-CoV-2 N-protein. To further substantiate the inhibition results in

vitro, the evaluation of the antiviral potency of the compounds was done via in vitro cell-based assays.

Antiviral efficacy against SARS-CoV-2

Cell viability studies of the selected compounds were carried out on Vero cells using MTT assay before performing the antiviral assay to determine the 50% cytotoxic concentration (CC_{50}) value of the compounds. CC_{50} value is defined as the drug concentration required to reduce cell viability by 50%. CC_{50} values for all compounds are shown in figure 6. DMSO was used as a vehicle control, and a statistically significant increase in cell cytotoxicity was observed when Vero cells were treated with increased concentrations of compounds. To assess the antiviral potential of selected compounds, Vero cells were treated with different concentrations of compounds before and after infection with SARS-CoV-2 (SARS-CoV-2/Human/IND/CAD1339/2020) at an MOI of 0.01. Cell culture supernatants were harvested at 48 hours post-infection (hpi), and the antiviral efficacies of the selected compounds were evaluated by quantifying viral RNA in the cell culture supernatant using qRT-PCR. Among the twelve drugs that were assessed in the present study, ten compounds displayed potential antiviral activities against SARS-CoV-2. EC_{50} of these compounds were determined using GraphPad Prism software. The EC_{50} values for the compounds were determined [Figure 6]. As elucidated from the qRT-PCR assay, treatment with the aforementioned compounds potently inhibited SARS-CoV-2 at a low micromolar range [Figure 6]. Apatinib and BMS 927711 were found to be the least effective at non-toxic concentrations, and the higher doses of these compounds were observed to be highly toxic. Interestingly, a recent report also corroborates our finding of Telmisartan(Micardis), an Angiotensin II type 1 (AT1) receptor antagonist, as a potential and effective antiviral drug against the treatment of SARS-CoV-2[49]. A strong inhibition pattern was observed for MCC 555, Bictegravir, ANA-12, Alisol_B, and Bisdemethoxycurcumin with a percentage inhibition of more than 90% at low concentrations and high concentrations of these compounds were able to suppress SARS-CoV-2 infection completely. To further confirm the antiviral efficacy of these four compounds on SARS-CoV-2, cell culture supernatants harvested from antiviral assays of these compounds were further subjected to end-point assay for $TCID_{50}$ determination.

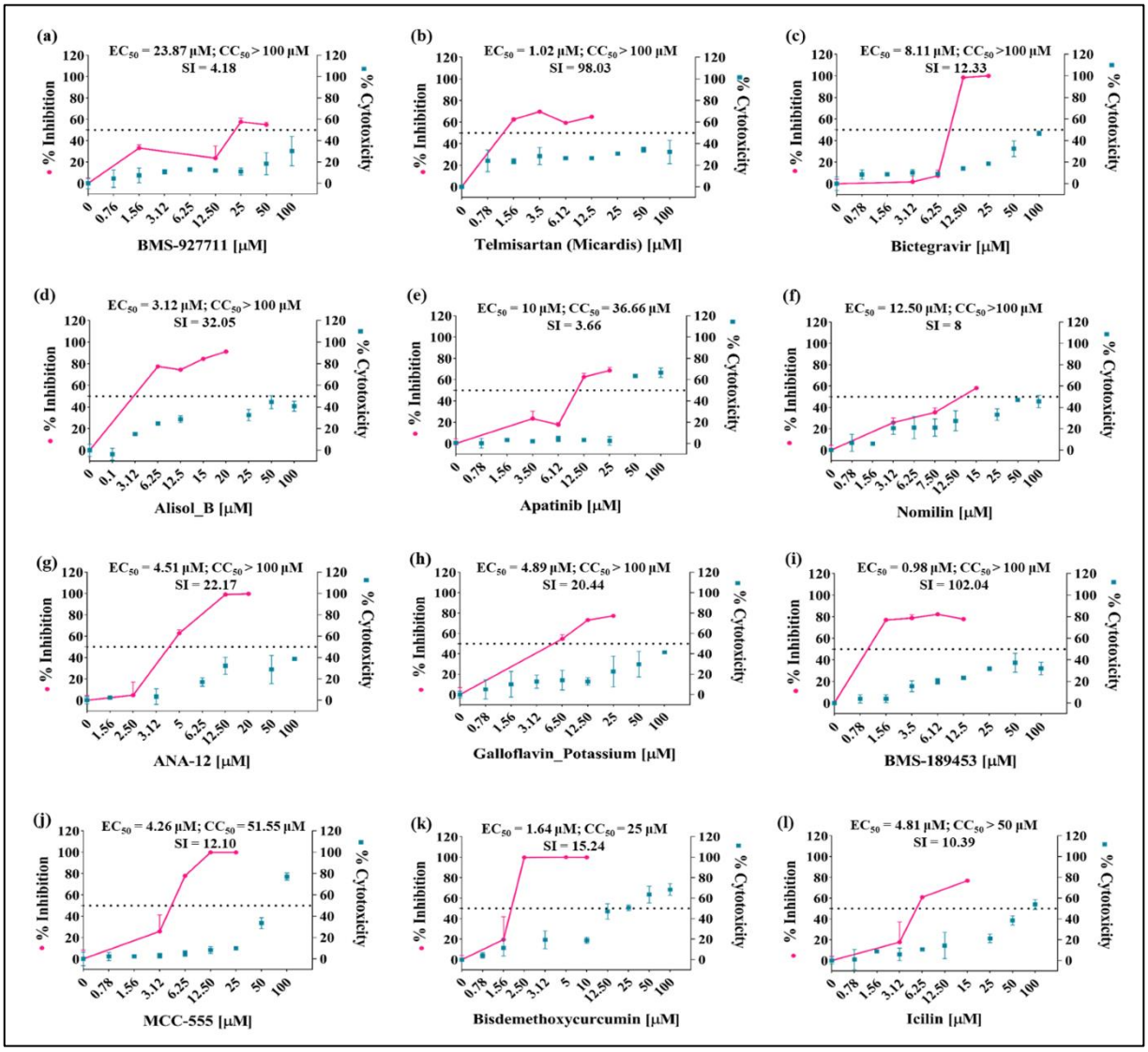

Figure 6. Anti-SARS-CoV-2 profiles of selected compounds. Vero cells were treated with different doses of compounds chosen before and after infection with SARS-CoV-2 (MOI 0.01). qRT-PCR quantified the viral yield in the presence and absence of compounds, and the percentage inhibition versus concentration graph was plotted. Results are representative of n = 2 and are shown as mean ± standard deviation. Cytotoxicity of these compounds was assessed using an MTT assay. The pink circles and lines specify the percentage inhibition of SARS-CoV-2 on treatment with selected compounds, and blue squares denote percentage cytotoxicity values at 48 hpi. The left and right Y-axis corresponds to percent inhibition and percentage cytotoxicity, respectively. The 50% cytotoxic concentration (CC_{50}), half maximal effective concentration (EC_{50}), and Selectivity Index (SI) values of each compound were calculated and displayed on each corresponding graph's upper panel. Values are mean, and error bars are standard deviations from duplicate reactions. The data were normalized, and CC_{50} and EC_{50} values were calculated using Graph Pad Prism's non-linear regression fit model.

In concordance with the antiviral assay, the compound-treated groups showed a significant decrease in viral titer in the $TCID_{50}$ assay than those of untreated virus control at non-toxic levels. The $TCID_{50}$/ml value observed for compound-treated groups was $10^{2.49}$ for MCC 555 at 25 µM, $10^{1.8}$ for Bictegravir at 25 µM, $10^{2.03}$ for Bisdemethoxycurcumin at 10 µM, and $10^{2.16}$ for ANA-12 at 20 µM in comparison to the virus control group ($10^{4.34}$ $TCID_{50}$/ml). The results obtained from the $TCID_{50}$ assay displayed a dose-dependent inhibitory

pattern of these four compounds against SARS-CoV-2. Taken together, these findings reveal the anti-SARS-CoV-2 activity of the tweleve compounds, predominantly by Telmisartan and BMS-189453.

Discussion

Identification of drug targeting sites in viral proteins is very crucial to develop antiviral therapy and combat the virus. This study utilizes the structural information available on the NTD of SARS-CoV-2 N-protein for virtual screening to identify potential antivirals using the drug molecule repositioning approach. Further, biophysical binding characterization and antiviral cell-based studies were performed to validate the inhibitory potential of identified molecules against the RNA-NTD molecular interactions, which are critical for the virus replication cycle. The N-protein, a major structural component of the virion, plays a crucial role in viral assembly, genome packaging, replication, transcription, and host immune response regulation by forming a ribonucleoprotein (RNP) complex[50]. Previous studies suggest that small molecules targeting the RNA-binding pocket of the N-terminal domain could suppress viral infection by hindering the interaction between the N-protein and viral RNA[13]. The detailed docking studies indicate that the molecules identified in this study interact at the reported RNA binding site SARS-CoV-2 N-protein[51] and found to have additional interactions that enhance their binding affinity towards the NTD. Overall, these molecules hold potential as inhibitors of SARS-CoV-2 replication by hindering the interaction between the N-protein and viral RNA. [Figure 1, 2, 3, and Table 1]. The identified small molecules targeting the RNA binding pocket of NTD were validated using ITC measurements, confirming their high binding affinities towards NTD with K_D values in the lower micromolar range. The KD values of the ligands ranged from 5.95 µM - 90 µM. [Figure 4 and Table 2]. The NTD-RNA binding assay showed the potential of the identified compounds to inhibit the interactions of NTD with viral genomic RNA[52] (Figure S3). The NTD-RNA binding assay showed high-affinity interaction between NTD and RNA. The selected compounds showed a significant inhibitory effect on this interaction, with a decrease in fluorescence intensity [Figure 5]. The antiviral potential of twelve selected ligands against SARS-CoV-2 was evaluated through cell-based in vitro assays after obtaining promising results from docking, biophysical, and fluorescence-based binding inhibition studies. The EC_{50} values of Telmisartan and BMS-189453 were found to be strong, with values ~1.0 µM and ~0.98 µM respectively. In contrast, Apatinib and BMS927711 were the least effective [Figure 7]. This study suggests a promising approach for developing antiviral therapy to combat emerging variants of SARS-CoV-2.

Interestingly, most of these compounds identified in this study are reported as anti-cancerous, anti-diabetic, and some are commercially available as antivirals [ST 1]. Therefore, this study identified effective anti-SARS-CoV-2 molecules that target the RNA binding pocket of NTD, with EC_{50} values ranging from 0.98 µM-23 µM. The identified compounds have the potential to be repurposed as monotherapy or combination therapy to fight against COVID-19 and future pandemic waves, and are expected to be effective against emerging variants. Further studies using relevant mouse models and subsequent human clinical trials are required to verify their efficacy.

Acknowledgements

P.K., R.K.P., G.K.S., and S.T. acknowledge and thank Science and Engineering Research Board, Department of Science & Technology, Government of India (Project no. IPA/2020/000054) for supporting this study. P.K. and S.T. also thank Department of Biosciences and Bioengineering (BSBE), Government of India, for supporting Bioinformatics Centre at IIT Roorkee (reference number BT/PR40141/BTIS/137/16/2021). P.D. and A.S. are supported by Ministry of Human Resource and Development (MHRD), Government of India for financial support. S.C. thanks Council of Scientific & Industrial Research (CSIR), Government of India for financial support. We also thank the Macromolecular Crystallographic Facility (MCU) at Indian Institute of Technology Roorkee (IIT Roorkee) for the computer facility. A preprint of this paper is available at bioRxiv[53]; doi: https://doi.org/10.1101/2022.03.12.484092.

Contributions

Contributions

Conceptualization, P.K., G.K.S., R.K.P., and S.T.; methodology, P.K., S.T., G.K.S., P.D., A.S., and S.C.; Experimentation, G.K.S., P.D., A.S., and S.C.; formal analysis, P.K., G.K.S., and S.T.; writing—original draft, P.D., A.S., and S.C., writing—review & editing, R.K.P., P.K., G.K.S., and S.T., supervision, P.K., G.K.S., and S.T.; funding acquisition, P.K., G.K.S., and S.T.; All authors read, revised and approved the manuscript.

Corresponding authors

Correspondence to Pravindra Kumar, Gaurav Kumar Sharma, Shailly Tomar

Ethics declarations

Competing interests

The authors declare no competing interests.

References

1. Omer EA, Abdelfatah S, Riedl M, Meesters C, Hildebrandt A, Efferth T. Coronavirus Inhibitors Targeting nsp16. *Mol 2023, Vol 28, Page 988* 2023; **28**: 988. Available at: https://www.mdpi.com/1420-3049/28/3/988/htm. Accessed June 26, 2023.
2. Ortiz-Prado E, Simbaña-Rivera K, Gómez- Barreno L, *et al.* Clinical, molecular, and epidemiological characterization of the SARS-CoV-2 virus and the Coronavirus Disease 2019 (COVID-19), a comprehensive literature review. *Diagn Microbiol Infect Dis* 2020; **98**: 115094.
3. Masters PS. The Molecular Biology of Coronaviruses. *Adv Virus Res* 2006; **66**: 193–292.
4. V T, KA I, Á P, *et al.* Mechanisms and enzymes involved in SARS coronavirus genome expression. *J Gen Virol* 2003; **84**: 2305–15. Available at: https://pubmed.ncbi.nlm.nih.gov/12917450/. Accessed September 4, 2021.
5. Hurst KR, Koetzner CA, Masters PS. Identification of In Vivo-Interacting Domains of the Murine Coronavirus Nucleocapsid Protein. *J Virol* 2009; **83**: 7221–34. Available at: https://journals.asm.org/journal/jvi. Accessed September 9, 2021.
6. Lu S, Ye Q, Singh D, *et al.* The SARS-CoV-2 nucleocapsid phosphoprotein forms mutually exclusive condensates with RNA and the membrane-associated M protein. *Nat Commun 2021 121* 2021; **12**: 1–15. Available at: https://www.nature.com/articles/s41467-020-20768-y. Accessed September 9, 2021.

7. Peng TY, Lee KR TW. Phosphorylation of the arginine/serine dipeptide-rich motif of the severe acute respiratory syndrome coronavirus nucleocapsid protein modulates its multimerization, translation inhibitory activity and cellular localization. *FEBS J* 2008; **275**: 4152–63. Available at: https://pubmed.ncbi.nlm.nih.gov/18631359/. Accessed September 9, 2021.
8. Grossoehme NE, Li L, Keane SC, *et al.* Coronavirus N Protein N-Terminal Domain (NTD) Specifically Binds the Transcriptional Regulatory Sequence (TRS) and Melts TRS-cTRS RNA Duplexes. *J Mol Biol* 2009; **394**: 544–57.
9. V'kovski P, Kratzel A, Steiner S, Stalder H, Thiel V. Coronavirus biology and replication: implications for SARS-CoV-2. *Nat Rev Microbiol 2020 193* 2020; **19**: 155–70. Available at: https://www.nature.com/articles/s41579-020-00468-6. Accessed October 6, 2022.
10. CK C, YL H, YH C, *et al.* Multiple nucleic acid binding sites and intrinsic disorder of severe acute respiratory syndrome coronavirus nucleocapsid protein: implications for ribonucleocapsid protein packaging. *J Virol* 2009; **83**: 2255–64. Available at: https://pubmed.ncbi.nlm.nih.gov/19052082/. Accessed September 9, 2021.
11. Kang S, Yang M, Hong Z, *et al.* Crystal structure of SARS-CoV-2 nucleocapsid protein RNA binding domain reveals potential unique drug targeting sites. *Acta Pharm Sin B* 2020; **10**: 1228–38.
12. Dhankhar P, Dalal V, Singh V, Tomar S, Kumar P. Computational guided identification of novel potent inhibitors of N-terminal domain of nucleocapsid protein of severe acute respiratory syndrome coronavirus 2. *https://doi.org/101080/0739110220201852968* 2020. Available at: https://www.tandfonline.com/doi/abs/10.1080/07391102.2020.1852968. Accessed September 14, 2021.
13. Lin SY, Liu CL, Chang YM, Zhao J, Perlman S, Hou MH. Structural basis for the identification of the N-terminal domain of coronavirus nucleocapsid protein as an antiviral target. *J Med Chem* 2014; **57**: 2247–57. Available at: https://pubs.acs.org/doi/full/10.1021/jm500089r. Accessed January 24, 2022.
14. Montes-Grajales D, Puerta-Guardo H, Espinosa DA, *et al.* In silico drug repurposing for the identification of potential candidate molecules against arboviruses infection. *Antiviral Res* 2020; **173**: 104668.
15. Rani R, Long S, Pareek A, *et al.* Multi-target direct-acting SARS-CoV-2 antivirals against the nucleotide-binding pockets of virus-specific proteins. *Virology* 2022; **577**: 1–15.
16. Meinhardt J, Radke J, Dittmayer C, *et al.* Olfactory transmucosal SARS-CoV-2 invasion as a port of central nervous system entry in individuals with COVID-19. *Nat Neurosci 2020 242* 2020; **24**: 168–75. Available at: https://www.nature.com/articles/s41593-020-00758-5. Accessed June 13, 2022.
17. Littler DR, MacLachlan BJ, Watson GM, Vivian JP, Gully BS. A pocket guide on how to structure SARS-CoV-2 drugs and therapies. *Biochem Soc Trans* 2020; **48**: 2625–41. Available at: /biochemsoctrans/article/48/6/2625/227086/A-pocket-guide-on-how-to-structure-SARS-CoV-2. Accessed June 26, 2023.
18. Souza BG de, Choudhary S, Vilela GG, *et al.* Design, synthesis, antiviral evaluation, and In silico studies of acrylamides targeting nsP2 from Chikungunya virus. *Eur J Med Chem* 2023; **258**: 115572. Available at: https://linkinghub.elsevier.com/retrieve/pii/S022352342300538X. Accessed June 26, 2023.
19. Choudhary S, Malik YS, Tomar S. Identification of SARS-CoV-2 Cell Entry Inhibitors by Drug Repurposing Using in silico Structure-Based Virtual Screening Approach. *Front Immunol* 2020; **0**: 1664.
20. Pareek A, Kumar R, Mudgal R, *et al.* Alphavirus antivirals targeting RNA-dependent RNA polymerase domain of nsP4 divulged using surface plasmon resonance. *FEBS J* 2022; **289**: 4901–24. Available at: https://onlinelibrary.wiley.com/doi/full/10.1111/febs.16397.

Accessed September 28, 2022.
21. Fatma B, Kumar R, Singh VA, *et al.* Alphavirus capsid protease inhibitors as potential antiviral agents for Chikungunya infection. *Antiviral Res* 2020; **179**: 104808.
22. Mudgal R, Mahajan S, Tomar S. Inhibition of Chikungunya virus by an adenosine analog targeting the SAM-dependent nsP1 methyltransferase. *FEBS Lett* 2020; **594**: 678–94. Available at: https://onlinelibrary.wiley.com/doi/full/10.1002/1873-3468.13642. Accessed September 14, 2021.
23. Hwang H, Kim H, Myong S. Protein induced fluorescence enhancement as a single molecule assay with short distance sensitivity. *Proc Natl Acad Sci U S A* 2011; **108**: 7414–8.
24. Byun WG, Lim D, Park SB. Discovery of Small-Molecule Modulators of Protein–RNA Interactions by Fluorescence Intensity-Based Binding Assay. *ChemBioChem* 2020; **21**: 818–24. Available at: https://onlinelibrary.wiley.com/doi/full/10.1002/cbic.201900467. Accessed September 26, 2022.
25. Robert X, Gouet P. Deciphering key features in protein structures with the new ENDscript server. *Nucleic Acids Res* 2014; **42**: W320–4. Available at: https://academic.oup.com/nar/article/42/W1/W320/2435247. Accessed March 8, 2022.
26. Corpet F. Multiple sequence alignment with hierarchical clustering. *Nucleic Acids Res* 1988; **16**: 10881. Available at: /pmc/articles/PMC338945/?report=abstract. Accessed March 8, 2022.
27. Saikatendu KS, Joseph JS, Subramanian V, *et al.* Ribonucleocapsid Formation of Severe Acute Respiratory Syndrome Coronavirus through Molecular Action of the N-Terminal Domain of N Protein. *J Virol* 2007; **81**: 3913–21. Available at: https://journals.asm.org/doi/abs/10.1128/JVI.02236-06. Accessed March 8, 2022.
28. Papageorgiou N, Lichière J, Baklouti A, *et al.* Structural characterization of the N-terminal part of the MERS-CoV nucleocapsid by X-ray diffraction and small-angle X-ray scattering. *urn:issn:2059-7983* 2016; **72**: 192–202. Available at: http://scripts.iucr.org/cgi-bin/paper?mn5105. Accessed September 9, 2021.
29. Delano WL. PyMOL: An Open-Source Molecular Graphics Tool.
30. Morris GM, Huey R, Lindstrom W, *et al.* AutoDock4 and AutoDockTools4: Automated Docking with Selective Receptor Flexibility. *J Comput Chem* 2009; **30**: 2785. Available at: /pmc/articles/PMC2760638/. Accessed September 14, 2021.
31. Trott O, Olson AJ. AutoDock Vina: improving the speed and accuracy of docking with a new scoring function, efficient optimization and multithreading. *J Comput Chem* 2010; **31**: 455. Available at: /pmc/articles/PMC3041641/. Accessed January 24, 2022.
32. Laskowski RA, Swindells MB. LigPlot+: multiple ligand-protein interaction diagrams for drug discovery. *J Chem Inf Model* 2011; **51**: 2778–86. Available at: https://pubmed.ncbi.nlm.nih.gov/21919503/. Accessed January 24, 2022.
33. Dallakyan S, Olson AJ. Small-molecule library screening by docking with PyRx. *Methods Mol Biol* 2015; **1263**: 243–50.
34. Anon. LOPAC®1280. Available at: https://www.sigmaaldrich.com/IN/en/product/sigma/lo1280?gclid=Cj0KCQjw4eaJBhDMARIsANhrQAB1IuHF4JTei1ME1uaJQk5Pc024Y4gEsBbXwVKwbzVq2RVH8NgPcnAaAg-QEALw_wcB. Accessed September 9, 2021.
35. Anon. Caithness Biotechnologies - Focussed libraries for drug discovery. Available at: http://www.caithnessbiotechnologies.com/products.html. Accessed September 9, 2021.
36. Chang CK, Lo SC, Wang YS, Hou MH. Recent insights into the development of therapeutics against coronavirus diseases by targeting N protein. *Drug Discov Today* 2016; **21**: 562. Available at: /pmc/articles/PMC7108309/. Accessed June 26, 2023.
37. Wu W, Cheng Y, Zhou H, Sun C, Zhang S. The SARS-CoV-2 nucleocapsid protein: its role in the viral life cycle, structure and functions, and use as a potential target in the

development of vaccines and diagnostics. *Virol J 2023 201* 2023; **20**: 1–16. Available at: https://virologyj.biomedcentral.com/articles/10.1186/s12985-023-01968-6. Accessed June 26, 2023.
38. Vanommeslaeghe K, Hatcher E, Acharya C, *et al.* CHARMM General Force Field (CGenFF): A force field for drug-like molecules compatible with the CHARMM all-atom additive biological force fields. *J Comput Chem* 2010; **31**: 671. Available at: /pmc/articles/PMC2888302/. Accessed November 21, 2022.
39. Huang J, Rauscher S, Nawrocki G, *et al.* CHARMM36m: An Improved Force Field for Folded and Intrinsically Disordered Proteins. *Nat Methods* 2017; **14**: 71. Available at: /pmc/articles/PMC5199616/. Accessed November 21, 2022.
40. Anon. MicroCal iTC200 isothermal titration calorimeter from Malvern | Product support | Malvern Panalytical. Available at: https://www.malvernpanalytical.com/en/support/product-support/microcal-range/microcal-itc-range/microcal-itc200. Accessed January 24, 2022.
41. Anon. Welcome to Biotech Desk Pvt. Ltd. Available at: https://www.biotechdesk.com/. Accessed June 26, 2023.
42. Anon. Economical Multimode Microplate Reader, BioTek Synergy HTX | Agilent. Available at: https://www.agilent.com/en/product/microplate-instrumentation/microplate-readers/multimode-microplate-readers/biotek-synergy-htx-multimode-reader-1623207?Product_Interest_Source=Marketing Campaign&source=Marketing Campaign&Lead_Campaign_Source=7015Y000002uboQ&Campaign_Source=7015Y000002uboQ&utm_source=biotek&utm_medium=cpc&utm_campaign=7015Y000002uboQ&gad=1&gclid=Cj0KCQjw7uSkBhDGARIsAMCZNJuLbo1aukORKFGgen0xyjZm3LDXu3qY2EtCAcNlRpH8aqr62HNytHMaAgEIEALw_wcB&gclsrc=aw.ds. Accessed June 26, 2023.
43. Anon. Prism - GraphPad. Available at: https://www.graphpad.com/scientific-software/prism/. Accessed November 21, 2022.
44. Moghaddam E, Teoh BT, Sam SS, *et al.* Baicalin, a metabolite of baicalein with antiviral activity against dengue virus. *Sci Rep* 2014; **4**. Available at: https://pubmed.ncbi.nlm.nih.gov/24965553/. Accessed January 24, 2022.
45. Cao R, Hu H, Li Y, *et al.* Anti-SARS-CoV-2 potential of artemisinins in vitro. *ACS Infect Dis* 2020; **6**: 2524–31. Available at: /pmc/articles/PMC7437450/. Accessed January 24, 2022.
46. Wang M, Cao R, Zhang L, *et al.* Remdesivir and chloroquine effectively inhibit the recently emerged novel coronavirus (2019-nCoV) in vitro. *Cell Res 2020 303* 2020; **30**: 269–71. Available at: https://www.nature.com/articles/s41422-020-0282-0. Accessed January 24, 2022.
47. Reed LJ, Muench H. A simple method of estimating fifty per cent endpoints. *Am J Epidemiol* 1938; **27**: 493–7. Available at: https://academic.oup.com/aje/article/27/3/493/99616. Accessed January 24, 2022.
48. Peng Y, Du N, Lei Y, *et al.* Structures of the SARS-CoV-2 nucleocapsid and their perspectives for drug design. *EMBO J* 2020; **39**: e105938. Available at: https://www.embopress.org/doi/full/10.15252/embj.2020105938. Accessed September 9, 2021.
49. Duarte M, Pelorosso F, Nicolosi LN, *et al.* Telmisartan for treatment of Covid-19 patients: An open multicenter randomized clinical trial. *EClinicalMedicine* 2021; **37**. Available at: http://www.thelancet.com/article/S258953702100242X/fulltext. Accessed March 12, 2022.
50. Bai Z, Cao Y, Liu W, Li J. The SARS-CoV-2 Nucleocapsid Protein and Its Role in Viral Structure, Biological Functions, and a Potential Target for Drug or Vaccine Mitigation. *Viruses* 2021; **13**. Available at: https://pubmed.ncbi.nlm.nih.gov/34200602/. Accessed January 24, 2022.
51. Kang S, Yang M, Hong Z, *et al.* Crystal structure of SARS-CoV-2 nucleocapsid protein

RNA binding domain reveals potential unique drug targeting sites. *Acta Pharm Sin B* 2020; **10**: 1228. Available at: /pmc/articles/PMC7194921/. Accessed September 6, 2021.
52. Luan X, Li X, Li Y, *et al.* Antiviral drug design based on structural insights into the N-terminal domain and C-terminal domain of the SARS-CoV-2 nucleocapsid protein. *Sci Bull* 2022; **67**: 2327–35.
53. Anon. All Articles | bioRxiv. Available at: https://www.biorxiv.org/content/early/recent?page=8. Accessed March 15, 2022.